

# Evidence for Intermittent Turbulence from Scintillation Parameters of PSR J0437-4715

C. Hirano, C.R. Gwinn

*Department of Physics, University of California, Santa Barbara, CA 93106*

S. Boldyrev

*Institute for Theoretical Physics, University of California, Santa Barbara, CA 93106*

`placebo@condor.physics.ucsb.edu`

`cgwinn@condor.physics.ucsb.edu`

`boldyrev@itp.ucsb.edu`

## ABSTRACT

We propose a novel model for radio-wave scattering in the interstellar medium, on the basis of observations of PSR J0437-4715. We find that, although our estimates of the scintillation velocity and the distance to the scattering material agree with previous estimates, the decorrelation bandwidth and time scale of scintillation for this pulsar differ by an order of magnitude from those extrapolated from previous observations. We do, however, observe a small modulation that matches extrapolation. We propose that this modulation arises from strongly non-Gaussian statistics of the scattering process, leading to important contributions from both multiple deflections at small angles, and large, single deflections at large angles. A simple model for such scattering reproduces the observed fine-scale structure in scintillation spectra of PSR J0437-4715 and other low-dispersion pulsars, and the observed scaling of temporal broadening  $\tau_s$  with dispersion measure  $DM$  of  $\tau_s \propto DM^{4.4}$  for more distant pulsars.

*Subject headings:* pulsars: individual (PSR J0437-4715)

## 1. Introduction

Fluctuations in the electron density in the interstellar medium (ISM) scatter electromagnetic radiation from a source such as a pulsar, giving rise to the phenomenon of interstellar

scintillation (ISS). While some models explore scattering in an extended medium, simplified models typically assume that radiation from the source scatters off a thin screen located between the source and observer. Rays may reach an observer via multiple paths, and the resulting interference creates a diffraction pattern in the observing plane.

Scintillation causes the intensity of the source to vary with time and frequency. The time variations arise from motions of the source and screen relative to the observer which cause the scintillation pattern to move relative to the observer with scintillation velocity  $V_{ISS}$ . In the frequency domain, scintillation maxima have finite widths as the conditions which result in constructive interference at one frequency result in destructive interference at a sufficiently different frequency. The two observables, the scintillation time scale  $t_{ISS}$  and decorrelation bandwidth  $\Delta\nu_{ISS}$ , characterize the size of the maxima along the time and frequency dimensions of the dynamic spectrum of scintillation.

Models of the ISM predict how these observables scale with observing frequency  $\nu$ . For interstellar scattering, we expect  $\Delta\nu_{ISS} \propto \nu^{4.0 \text{ to } 4.4}$  and  $t_{ISS} \propto \nu^{1.0 \text{ to } 1.2}$ . In the Kolmogorov model, the power spectrum of the electron density fluctuations is given by

$$P(q) = C_n^2 q^{-11/3} \quad \frac{2\pi}{l_o} \leq q \leq \frac{2\pi}{l_i} \quad (1)$$

which holds between an inner length scale  $l_i$  and outer length scale  $l_o$ .  $C_n$  denotes the level of density fluctuations, and  $q$ , the wavenumber. With this model, we expect that  $\Delta\nu_{ISS} \propto \nu^{4.4}$  and  $t_{ISS} \propto \nu^{1.2}$ .

### 1.1. Scintillation Velocity

One can find the scintillation velocity  $V_{ISS}$  via the relation (Gupta et al. 1994)

$$V_{ISS} = A_V \frac{\sqrt{\Delta\nu_{\text{MHz}} D_{\text{kpc}} x}}{\nu_{\text{GHz}} t_{ISS}} \text{ km s}^{-1}. \quad (2)$$

Here  $\Delta\nu_{\text{MHz}}$  is the decorrelation bandwidth in megahertz;  $D_{\text{kpc}}$  is the distance to the pulsar in kiloparsecs;  $t_{ISS}$  is the scintillation time scale in seconds; and  $\nu_{\text{GHz}}$  is the observing frequency in gigahertz. Traditionally, the parameter  $x = d_s/(D - d_s)$ , where  $D$  is the observer-to-pulsar distance and  $d_s$  is the observer-to-screen distance, is taken to be unity; in other words, the scattering screen is assumed to be halfway between the observer and the pulsar. The numerical factor  $A_V$  is a model-dependent constant. Lyne & Smith (1982) used a value of  $2 \times 10^4$  while Cordes (1986) and Harrison & Lyne (1993) used a value of  $1.27 \times 10^4$ . Gupta et al. (1994) subsequently derived a new estimate for  $A_V$  of  $3.85 \times 10^4$ , which is the value we adopt in our analysis.

From the scintillation velocity  $V_{ISS}$ , one can infer the velocity of the pulsar using a lever-arm argument. Studies by Lyne & Smith (1982), Cordes (1986), and Gupta et al. (1994) compared velocities derived from scintillation methods with those measured using other methods and found the two sets of results were correlated. Scintillation methods, however, systematically underestimated the proper motion of pulsars (Harrison & Lyne 1993). Gupta (1995) reexamined the correlation using the revised value of  $A_V$  and taking into account revisions to the pulsar distance scale (Taylor & Cordes 1993) and found that the systematic bias disappeared and that the two sets of results agreed quite well statistically.

The broadening time  $\tau_s$  and the decorrelation bandwidth  $\Delta\nu_{ISS}$  are related via the uncertainty relation

$$\Delta\nu_{ISS} \tau_s = \frac{C_1}{2\pi}, \quad (3)$$

where the constant  $C_1$  depends on the scattering model and on the particular definitions of  $\Delta\nu_{ISS}$  and  $\tau_s$ . For their pulsar catalog, Taylor, Manchester, & Lyne (1993) used a value of  $C_1 = 1.53$ . Lambert & Rickett (1999) subsequently argued that for a thin-screen geometry this value of  $C_1$  results in overestimates of the broadening time by a factor of 2.34. We therefore use  $C_1 = 0.654$  in our analysis.

Simple scattering models suggest that temporal broadening should depend approximately quadratically on dispersion measure  $DM$  (Sutton 1971). These models appeal to the random-walk character of scattering: one scattering will introduce a mean square deflection  $\Delta\theta^2$ , and  $N$  such deflections will produce mean square deflection  $\theta_1^2 \sim N\Delta\theta^2$ . The geometrical relation  $c\tau_s \sim \theta_1^2 D$ , and the plausible assumption that  $DM \propto D \propto N$ , then yield  $\tau_s \propto DM^2$ . Observations agree with this scaling for small dispersion measures; however, for large dispersion measures,  $\tau_s \propto DM^{4.4}$ , as shown in Figure 1 (Lyne & Graham-Smith 1998). The cutoff between the two regimes appears around  $DM \approx 30 \text{ cm}^{-3} \text{ pc}$ .

Recently, Boldyrev & Gwinn (2002) proposed that Levy flights could provide a satisfactory model for interstellar radio-wave propagation. For both Levy flights and random walks with Gaussian steps, the distribution remains identical, with appropriate scaling, as the path is extended. However, Levy flights are dominated by large, rare excursions and the distributions are far from Gaussian, with much higher wings. Boldyrev & Gwinn (2002) show that Levy flights can reproduce the observed scaling  $\tau_s \propto \lambda^{4.0 \text{ to } 4.4} DM^{4.0 \text{ to } 4.4}$ . Levy flights are expected for turbulent media. Interestingly, Sutton (1971) appealed to rare, large events to explain the observed scaling as well, although he appealed to macroscopic events: increasing probability of intersecting a stronger scattering region, with increasing length of the line of sight. In this paper, we explore how Levy flights might explain the multiple scales of scattering we observe for PSR J0437-4715.

## 2. Observations and Analysis

### 2.1. Data Collection and Calibration

With its low dispersion measure of  $DM = 2.6484 \text{ cm}^{-3} \text{ pc}$ , PSR J0437-4715 lies at left end of Figure 1, providing us with one compelling reason to observe this particular pulsar, as we were interested in seeing if the pulsar followed the trend of other low- $DM$  pulsars. PSR J0437-4715 also has a well-defined bow shock (Fruchter 1998), and its strength and proximity, at a distance of 180 pc (Sandhu et al. 1997), make it a good candidate to probe the local ISM. The bow shock and the surface of the Local Bubble are two regions which could conceivably dominate the scattering behavior of the pulsar (Britton 1997).

We observed PSR J0437-4715 at two epochs using the Very Long Baseline Array (VLBA) operated by the National Radio Astronomy Observatory (NRAO). On 5 November 1996, we observed the pulsar over four 33-minute scans, using 25-meter telescopes at Fort Davis, Mauna Kea, Pie Town, and St. Croix, with a 32-MHz bandwidth centered at 332 MHz, and with a 250-kHz spectral resolution. Between the scans, we observed extragalactic sources for calibration purposes. On 8 April 1999, we observed the target for two 44-minute scans and one 33-minute scan, using the telescopes at Fort Davis, Kitt Peak, Los Alamos, Mauna Kea, Owens Valley, Pie Town, and St. Croix, with a bandwidth of 32 MHz centered at 328 MHz, and with a spectral resolution of 125 kHz. To increase the signal-to-noise ratio, the data for this observation were correlated using a gate which covered 12% of the pulse period and which isolated the central peak of the pulse profile. Scans of a calibrator source preceded and succeeded the observations of the pulsar. For both observations, we aggregated the 32-MHz bandwidth using four 8-MHz intermediate-frequency (IF) bands.

We performed half of the calibration using NRAO’s Astronomical Image Processing System (AIPS). The data from both observations were marred by radio-frequency interference (RFI). The second observation in particular suffered badly from RFI, forcing us to eliminate the Kitt Peak and Owens Valley antennas from the outset. The interference also tainted some of the measurements of the system temperature. The system temperature should not change abruptly, so if an isolated reading clearly departed from an otherwise smooth trend, we merely removed that value. In two IFs, however, rampant corruption due to RFI obliterated evidence of a smooth evolution in system temperature. For these two IFs, we copied the system temperatures from an adjacent IF, as system temperatures should not vary wildly from IF to IF.

We examined the remaining visibilities and flagged channels and time ranges to eliminate data corrupted by very strong, narrow-band signals typical of man-made sources. We applied the usual corrections for the effects of antenna parallactic angles, digital sampler bias, system

temperature, and gain calibration. We then performed a manual phase calibration by running a fringe fit on a thirty-second interval of calibrator data to determine the electronic delay differences between IFs, and we removed the resulting phase differences from the pulsar and calibrator data. The final procedure done using AIPS was a fringe fit on each source to remove phase slopes due to the residual fringe rate and delay.

To perform a bandpass calibration, we averaged, for each baseline, the complex visibilities from a ten-minute interval of calibrator data. Deviations from a flat amplitude and phase spectrum reflected the non-ideal frequency response of the baseband converters. The gain of the filters drops off at the ends of each IF, significantly reducing the signal-to-noise ratio in the first and last channel of each IF; consequently, we omitted these channels in our subsequent analysis. We then smoothed the data using boxcar averaging with a one-minute window to further increase the signal-to-noise ratio.

At our observing frequency, propagation through the ionosphere significantly affects the visibility phases (Thompson, Moran, & Swenson 1986). The fringe fit to remove the residual fringe rate eliminated the linear dependence of phase on time, but significant higher-order terms remained. Data from both observations exhibited broadband variations in phase of order half a radian over a time scale of about fifteen minutes, as would be expected for weak scattering in the ionosphere. We approximated and removed these variations using an eighth-order polynomial fit to amplitude-weighted phase averages calculated for each time point.

The ionosphere also induced phase curvature in frequency. The fringe fit removes the first-order dependence of phase on frequency, and usually, the bandwidth is small enough compared to the observing frequency that the second-order term is not important. However, in our case, the bandwidth was approximately 10% of the observing frequency, and the resulting 1% second-order correction could be of order a radian for typical values of total electron content for the ionosphere. We fit the amplitude-weighted phase averages calculated for each channel to a quadratic polynomial and used this polynomial to calculate the appropriate phase to subtract from the visibilities in each channel.

To verify that our calibration procedure did not introduce any unintended biases, we calculated two-dimensional autocorrelation functions (ACF) for each data set using the visibilities from a calibrator source. As expected, we obtained results flat in both time and frequency lags, except for a spike at small time and frequency lags due to the effects of noise, broadened from a delta-function by smoothing.

## 2.2. Observational Results

Initially, we had hoped to measure the angular broadening of the pulsar by measuring the phase variations of the diffraction pattern; however, several complications derailed our efforts. Most significantly, the decorrelation bandwidth was much larger than expected. As the phase variations of the diffraction pattern have this characteristic bandwidth (Desai et al. 1992), they could not be distinguished from ionospheric phase, phase slope, and curvature. Furthermore, we did not obtain fringes on the longest baseline where we expect phase variations of the diffraction pattern to be largest.

The remaining baselines were of comparable lengths, so we chose to focus on the Fort Davis-Pie Town baseline. Figure 2 shows plots of the visibility amplitudes for the pulsar on this baseline for both epochs. The white vertical lines correspond to the channels omitted at the ends of each IF, and the white horizontal lines correspond to breaks in the scan or to time ranges flagged because of RFI. At both epochs, we detected scintillation maxima that typically persist for ten to twenty minutes and that span several IFs, suggesting a characteristic width in frequency on the order of ten megahertz.

Gwinn et al. (1998) showed that for a Gaussian spectrum of density fluctuations, the ACF for zero time lag on a baseline of length  $b$  has the form

$$\langle C^*(\nu, t)C(\nu + \Delta\nu, t) \rangle \propto \bar{V}(b)^2 + \frac{1}{1 + (\Delta\nu/\Delta\nu_{ISS})^2} \quad (4)$$

where  $\bar{V}(b) = \exp[-(k\theta_1 b)^2/2]$  is the average normalized visibility. Here  $k$  is the wavenumber, and  $\theta_1$  is the angular size of the scattering disk, which is of order milliarcseconds. The length scale  $1/k\theta_1$  is of order  $10^4$  km and is larger than the diameter of the Earth; in particular, it is much greater than 565 km, the length of the Fort Davis-Pie Town baseline. Hence,  $k\theta_1 b \ll 1$  and

$$\langle C^*(\nu, t)C(\nu + \Delta\nu, t) \rangle \propto 1 + \frac{1}{1 + (\Delta\nu/\Delta\nu_{ISS})^2} \quad (5)$$

The small deviations from this form for a Kolmogorov or other plausible non-Gaussian spectrum would not affect our fitted results.

To determine the scintillation parameters, we calculated the two-dimensional ACFs for the Fort Davis-Pie Town baseline. Figure 3 shows the amplitude of one such ACF, with the noise spike removed. The contours divide the range of the function into ten equally sized intervals. We fit the time-lag axis of the two ACFs to the form given in equation (5). To each point used in the fit, we assigned a weight equal to the square root of the number of pairs used to calculate that point. The fits yielded a decorrelation bandwidth of  $14.7 \pm 0.5$  MHz for the first epoch and  $16.5 \pm 0.5$  MHz for the second. The uncertainties represent the 95%-confidence level of the fits.

Neither epoch individually provided a correlation function with a form particularly close to that given in equation (5); however, the composite ACF obtained by suitably combining the two individual functions did. To combine the two functions, we first halved the spectral resolution of the second-epoch function by averaging two adjacent bins, weighted according to the number of contributing pairs, into one bin, and then we averaged the two ACFs together bin by bin, again assigning weights proportional to the number of pairs contributing to a bin. The resulting function, shown in Figure 4, matched the theoretical prediction well. The solid curve shows the best-fitting Lorentzian, from which we obtained a decorrelation bandwidth of  $15.7 \pm 0.2$  MHz. Again, the uncertainty represents a 95%-confidence level for the fit.

To estimate the scintillation time scale, we fit the correlation function along the time-lag axis to a Gaussian plus an offset. The parameters of the fit were the offset and the amplitude and width of the Gaussian. The scintillation time scale is traditionally defined to be the time at which the Gaussian component of the correlation function declines to  $1/e$  of its maximum value. The fits yielded estimates of  $885 \pm 9$  s for the first epoch,  $1630 \pm 80$  s for the second, and  $1020 \pm 70$  s for the composite ACF.

Fits to correlation functions generated from simulated scintillation spectra with similar spans in time and frequency suggest fractional errors of about 20%, for our estimates of the correlation function. Gwinn et al. (1998) describe the simulation technique. This is in approximate accord with estimates from counting statistics, which suggest an error of approximately 20%, from the  $\approx 25$  independent samples in our (3.7 hr  $\times$  32 MHz) data set. Our simulations suggest that the distribution of errors is somewhat skew, with significant underestimates of the decorrelation bandwidth and scintillation timescale somewhat more likely than significant overestimates. We note, however, that the scintillation parameters are certainly far from those expected on the basis of scaling from previous observations, for which we would expect scintillation bandwidth and timescale corresponding to 1 or 2 pixels in Figure 2.

### 3. Discussion

#### 3.1. Scintillation Velocity

Using equation (2) with  $x = 1$  and  $D_{\text{kpc}} = 0.180$ , we calculated a scintillation velocity of  $V_{\text{ISS}} = 192$  km s $^{-1}$ , which agrees with previous measurements of the scintillation velocity. Johnston, Nicastro, & Koribalski (1998) obtained a value of 170 km s $^{-1}$  from observations at 436 MHz, and Gothoskar & Gupta (2000) measured a mean scintillation velocity of 231 km s $^{-1}$  from observations at 327 MHz. Proper motion measurements, however, have

yielded significantly lower results. Bell et al. (1995) found a velocity of  $91 \pm 3 \text{ km s}^{-1}$ , and Toscano et al. (1999), using arrival-time methods, recently obtained a velocity measurement of  $120.5 \pm 0.2 \text{ km s}^{-1}$ . This disparity suggests that the assumption that  $x = 1$ , that the scattering occurs midway between the source and observer, is not valid for PSR J0437-4715.

With the accuracy of scintillation methods established from measurements on other pulsars, we used this disparity to infer the distance to the scattering screen. The proper motion velocity of the pulsar  $V_{pm}$ , the scintillation velocity  $V_{ISS}$  (for  $x = 1$ ), and the relative location of the scattering screen are related by

$$\left(\frac{V_{ISS}}{V_{pm}}\right)^2 \approx x = \frac{d_s}{D - d_s}, \quad (6)$$

under the assumption that the velocity of the scattering material is negligible. Setting  $V_{pm} = 120.5 \text{ km s}^{-1}$ , we find that the scattering material is located at a distance  $d_s = 129 \text{ pc}$ .

Gothoskar & Gupta (2000) likewise noted that the scintillation velocity for PSR J0437-4715 significantly exceeds the proper motion of the pulsar, and that this fact indicates that the scattering occurs relatively close to the pulsar. Their analysis suggests that the scattering primarily occurs on the shell of the Local Bubble, which, they estimate, lies at a distance of approximately 120 pc along this line of sight. Our estimate of the distance to the scattering screen agrees well with their hypothesis.

### 3.2. Scintillation Bandwidth

#### 3.2.1. Comparison With Previous Results for PSR J0437-4715

Although our estimate for the scintillation velocity agrees well with previously reported results, our measurements of the decorrelation bandwidth  $\Delta\nu_{ISS}$  and scintillation time scale  $t_{ISS}$  do not. Figure 5 shows measurements of these two observables for observations of PSR J0437-4715, rescaled to an observing frequency of 330 MHz, versus observation date. The horizontal lines indicate the equivalent observing bandwidth for each measurement. Our estimates of  $\Delta\nu_{ISS}$  agree with a decorrelation bandwidth of  $0.5 \pm 0.1 \text{ MHz}$  at 150 MHz obtained by Issur (2000), but they clearly do not agree with the results reported by Nicastro & Johnston (1995), Johnston, Nicastro, & Koribalski (1998), and Gothoskar & Gupta (2000). Our estimates of the scintillation time scale are also inconsistent with earlier measurements.

Gothoskar & Gupta (2000) observed at 327 MHz, so we may rule out the possibility that the observables scale differently with frequency than expected as an explanation for the disagreement. Another possibility is that the nature of the scattering changes significantly

with time. Bhat (1999) observed that scintillation parameters often vary with time. Pulsars generally move with high speeds and therefore the line of sight to a pulsar may pass through regions of widely varying electron density on relatively short time scales.

Observations of PSR J0437-4715 arguably do not support this hypothesis. Gothoskar & Gupta (2000) found a decorrelation bandwidth of 1.56 MHz, consistent with the earlier results, from data taken 130 days after our first observation. Such a significant change over this time period would suggest that the scattering occurs in a small region close to the pulsar, yet Nicastro & Johnston (1995) observed PSR J0437-4715 at 436 MHz at five epochs over a 488-day period and did not see a dramatic shift in the decorrelation bandwidth.

A more intriguing possibility is that we are measuring different parameters than those in the earlier observations. The effective bandwidth of earlier observations corresponds to the width of one of our IFs, and as seen in Figure 5, our points lie outside this bandwidth because, as seen in Figure 2, a scintillation maximum typically spans several IFs. If the decorrelation bandwidth scales as expected with observing frequency, the earlier experiments may have detected evidence of structure within an intensity maximum that covered the entire observing bandwidth.

VLBI observations have an advantage over single-dish observations in these cases. In VLBI, because the receiver noise of the antennas are independent of each other, the average visibility will vanish when the signal vanishes; hence, we can easily tell whether or not the scintillation intensity goes to zero even when the intensity maximum encompasses nearly the entire bandwidth. In single-dish experiments, the receiver noise must be manually separated from the signal, allowing for the possibility that part of the signal is misidentified as noise.

### 3.2.2. *Fine-scale Structure Within Scintillation Maxima*

Figure 6 shows an expanded view of a scintillation maximum. The amplitude varies with a modulation index of  $m_f \approx 0.2$ , and the variations appear to occur with a characteristic bandwidth of  $\Delta\nu_f \sim 1$  MHz and on a time scale of a few minutes. Interestingly, these figures would agree with the estimates of the scintillation bandwidth and time scale from the earlier observations.

To verify the existence of a second characteristic scale, we focused on the most prominent intensity maximum from each observation, treating the two subsets of data individually. In both cases, we did not apply Hanning smoothing to the data to avoid obscuring evidence of the smaller scale. The component of the visibility due to the large scale modulation overwhelms the component responsible for the small scale modulation, in calculations of the

autocorrelation function, so we subtracted off the average visibility first to enhance effects of any small-scale correlations. The two resulting autocorrelation functions, one of which is shown in the upper plot in Figure 7, revealed correlations on scales of  $\Delta\nu_f = 0.6$  MHz and 0.4 MHz. To verify that these results were not artifacts of the analysis method, we applied the same procedure to data from the calibrator source. The result, shown in the lower plot, exhibits no evidence of correlation. In both plots, the spike due to noise at zero lag has been removed.

The time averaging required to increase the signal-to-noise ratio unfortunately smears the noise spike in the autocorrelation function, obscuring some evidence of correlation at small time lags. The upper plot in Figure 8 reveals correlations on a time scale of order one to two minutes for the first-epoch maximum. The autocorrelation function calculated for the other epoch from the un-Hanning-smoothed data did not show any evidence of correlation; however, using smoothed data revealed correlations at small time lags, again on the order of one to two minutes, as seen in the lower plot.

These results agree roughly with the earlier measurements of the scintillation bandwidth and time scale, but they tend toward smaller values. The measurements at 436 MHz and 660 MHz by Johnston, Nicastro, & Koribalski (1998) scale respectively to 1.1 MHz and 0.82 MHz at 330 MHz, and, as noted earlier, Gothoskar & Gupta (2000) found a decorrelation bandwidth of 1.56 MHz at an observing frequency of 327 MHz. Their reported values for  $t_{ISS}$ , appropriately rescaled, range from three to eight minutes, except for one value at just under two minutes.

Scattering can have more than one characteristic decorrelation bandwidth, as is the case for the Crab pulsar. Scattering of this pulsar by its supernova remnant and by the ISM along the line of sight produces two characteristic pulse broadening times (Lyne & Thorne 1975; Isaacman & Rankin 1977). PSR J0437-4715 could exhibit similar behavior; scattering may occur, for instance, at its bow shock and at the surface of the Local Bubble. However, the small characteristic bandwidth and small modulation index we found suggests that this is not the case: the small bandwidth suggests strong scattering while the small modulation index suggests weak scattering.

Interference between multiple images in the observing plane may explain the presence of fine structure. Cordes & Wolszczan (1986) and recently Stinebring et al. (2001), for example, have shown that multiple imaging of pulsars accounts for secondary features, such as multiple drift slopes, in pulsar dynamic spectra, and Gupta et al. (1999) have even analyzed these secondary features for PSR B1133+16 to infer the size of the pulsar’s emission region. The Fourier transform of the autocorrelation function reveals telltale attributes of this phenomenon; however, such an analysis of our data did not exhibit these attributes, probably

because of our limited amount of data.

Alternatively, the fine structure we see may be the result of a different mechanism altogether. We suggest in § 3.3 below that the fine structure arises from the unconverged part of a Levy distribution of scattering angles. In this picture, small angular deflections are common and lead to the fundamental scattering properties, realized in the case of PSR J0437-4715 by the broad scintillation bandwidth we measure,  $\Delta\nu = 16$  MHz. Large angular deflections are rare, but present; they lead to long paths and large time delays. These long paths interfere with the shorter ones, to produce narrow features in the scintillation spectrum. These lead to the finer-scale structure with modulation index less than 1, with characteristic bandwidth  $\Delta\nu_f \approx 0.5$  MHz.

### 3.2.3. Temporal Broadening of Nearby Pulsars

Our estimate of the decorrelation bandwidth corresponds to a broadening time  $\tau_s$  of  $5.0 \times 10^{-11}$  s at 1 GHz. (Because  $\tau_s$  is less than the wave period at 1 GHz,  $\tau_s$  should be viewed simply as a parameter and not the actual pulse broadening observable at that frequency.) As seen in Figure 1, our relatively large result for the decorrelation bandwidth and consequently small estimate of the broadening time moves PSR J0437-4715, despite its small dispersion measure, significantly toward the trend followed by pulsars with large dispersion measures; the previous estimates, in contrast, suggest that the pulsar behaves like a typical low-*DM* pulsar.

PSR B0950+08, which has a dispersion measure of  $2.9702 \text{ cm}^{-3}$  pc, also follows the trend of pulsars with large dispersion measures, based on measurements by Phillips & Clegg (1992). Observing at 47 MHz and 51 MHz, they also found a decorrelation bandwidth much larger than expected and attributed underestimates of the decorrelation bandwidth at higher frequencies to insufficient observing bandwidth at those frequencies.

For both PSR B0950+08 and PSR J0437-4715, observations at lower frequencies and wider bandwidth resulted in sharp upward revisions of the decorrelation bandwidth, leading to sharp downward revisions of the inferred temporal broadening  $\tau_s$ . For PSR B0950+08, earlier observations had reported intensity variations with frequency and time that varied greatly between observing epochs and often did not resemble that expected from scintillation (Armstrong & Rickett 1981; Roberts & Ables 1982; Cordes et al. 1985; Smirnova & Shabanova 1992). Phillips & Clegg (1992), with observations at 50 MHz, showed that these variations were much narrower in bandwidth and shorter in time scale than the actual scintillations. Similarly, for PSR J0437-4715, we describe above how observations at

higher frequencies and narrower bandwidth may have misinterpreted fine structure within the diffraction pattern as scintillations.

We suggest that other pulsars with low dispersion measure may have temporal broadening significantly smaller than represented in the literature and in Figure 1, and that this systematic overestimation of temporal broadening may explain the change in power-law index visible as a change in slope on the log-log scale of Figure 1. Bhat (1999) found that the measured decorrelation bandwidths of nearby pulsars varied greatly in time, by as much as an order of magnitude. Stinebring et al. (2001) find that fine structure in the scintillation spectrum occurs commonly among nearby pulsars.

For low- $DM$  pulsars, temporal broadening must be inferred from measurements of the decorrelation bandwidth. If structure with a variety of scales is present, observations, particularly if they are restricted to higher frequencies and narrower bandwidths by instrumental limitations, may tend to pick out the narrowest structures. As Figure 9 shows, misidentification of this fine structure as the fundamental scintillation pattern would result in underestimates of the decorrelation bandwidth and overestimates of the temporal broadening. On the other hand, observations of temporally-broadened pulses would tend to pick out the narrowest structures in time, which would correspond to the broadest scale of structure in the scintillation spectrum. Any fine structure would appear as a long tail on the scattered pulse, which might be difficult to distinguish from noise. Indeed, Sutton noted that the change from one technique to the other appeared precisely at the break in the scaling law in the Figure 1. We propose that these effects of fine structure in the scintillation might provide an instrumental explanation for the “kink” in that figure.

### 3.3. Levy Flights in Interstellar Propagation

#### 3.3.1. Turbulence, Intermittency, and Levy Flights

We propose a novel explanation for the fine structure seen in scintillations of PSR J0437-4715, PSR B0950+08, and other nearby pulsars. We suggest that the structure reflects scattering by non-Gaussian density fluctuations. Such “intermittent” statistics are common to many modern theories of turbulence (Frisch 1995). Intermittency reflects the fact that turbulence, and the structures that dissipate turbulent energy, may occupy only a fraction of space. They commonly lie on regions of fractal dimension less than 3. As Boldyrev & Gwinn (2002) propose, the effects of non-Gaussian fluctuations may be described by Levy statistics. In this picture, at a particular location the deflection angle  $\Delta\theta$  is drawn from a Levy distribution  $P(\Delta\theta)$ . Like a Gaussian distribution, the Levy distribution has

the property that the sum of successive draws from the distribution has the same form as the original distribution, suitably rescaled. However, the Levy distribution involves rare, large events that dominate at large values, and lead to much higher wings than a Gaussian distribution.

Boldyrev & Gwinn (2002) pointed out that a Levy flight with parameters  $\alpha = 0.67$  to  $1.0$  and  $\beta = 0.6$  to  $0.8$  reproduces the relations for angular broadening  $\theta_1 \propto \lambda^{2.0 \text{ to } 2.2} d^{0.5 \text{ to } 0.6}$  and for temporal broadening  $\tau_s \propto \lambda^{4.0 \text{ to } 4.4} d^{4.0 \text{ to } 4.4}$ , as observed for distant pulsars. In particular, for the parameters  $\alpha = 1$  and  $\beta = 2/3$ , we recover  $\tau_s \propto \lambda^4 D M^4$ . In these expressions,  $\alpha$  describes the decorrelation of density fluctuations with position, and is thus analogous to index characteristic of the Kolmogorov theory, which predicts  $\alpha = 2/3$ . (Note here that  $\alpha$  is not the power-law index of the structure function, because the second moment, and the structure function, do not exist.) The parameter  $\beta$  is  $2$  for a Gaussian distribution of density fluctuations, and  $\beta < 2$  for a Levy flight.

### 3.3.2. *Observations of Levy Flights*

For a Levy flight at small angles, the observed deflection is the consequence of small deflections that are likely, given the underlying distribution of scattering angles  $P(\Delta\theta)$  and the length of the line of sight. The medium can thus be viewed as optically thick at these small angles: deflection by these amounts is likely. On the other hand, radiation that reaches the observer from larger angles has suffered a rare, large deflection. Such deflections dominate the higher moments of  $P(\Delta\theta)$  but are nevertheless quite uncommon. For sufficiently large angles, the probability of any ray suffering the deflection required to reach the observer is much less than one. The medium can thus be seen as optically thin at these large angles.

The broadening time  $\tau_s$  is “fundamental” in the sense that it is the characteristic time for waves that propagate through the region of high optical depth. This time corresponds to the maximum scale of the scintillation spectrum,  $\Delta\nu_{ISS} = 1/(2\pi\tau_s)$ . It also corresponds to the minimum scale of temporal broadening, as shown in Figure 9.

Relatively rare, but large, deflections appear for sources at all distances, as a consequence of strongly-scattering clumps that are outside the zone where  $\tau = 1$ . Such large deflections would produce long path lengths, and thus might be responsible for the fine structure we observe in the scintillation spectra of PSR J0437-4715, and which others observe in PSR B0950+08 and other nearby objects. This structure can be expected to be highly time-variable, as Bhat (1999) found, and might be observed at wavelengths either where the “fundamental” scintillation is broader than the bandwidth of the observing sys-

tem, or where the “fundamental” scintillation is less than the wave period. In the latter case, interference among paths through the optically-thick region will produce only small intensity variations, whereas interference of those paths with highly-deflected ones can still result in large variations.

An interferometer will weight the bulk of the intensity most heavily, and will tend to observe only the central, optically-thick part of the scattered source. This could explain the observation of Britton, Gwinn, & Ojeda (1998) that scattered pulsars with low  $DM$  show undetectable angular broadening, significantly less than that predicted by their decorrelation bandwidths.

For PSR J0437-4715, the observed fine structure with  $\Delta\nu_f \approx 0.03\Delta\nu$  corresponds to scattering through an angle about  $1/\sqrt{0.03} \approx 6$  times greater than that of the optically-thick scattering. The modulation index for the fine structure of  $m_f \approx 0.2$  requires that the large-angle scattering involve a fraction of the power of the radiation  $\Delta I_f/I \sim m_f^4/(1 - \sqrt{1 - 2m_f})^2 \sim 0.03$  (or less if several highly-deflected paths contribute). The relatively strong modulation from a small fraction of scattered intensity reflects the interference of the large-angle and small-angle scattering.

### 3.3.3. Summary: Consequences of Levy Flights

We have proposed a simple model for the narrow-band substructure and the broader scintillation bandwidth of PSR J0437-4715. In this model, radio waves from radio sources are scattered through large angles with large, non-Gaussian, probability. The density fluctuations causing such large angle deviations could be governed by Levy statistics (as proposed by Boldyrev & Gwinn (2002)). One can demonstrate that the Levy model of scintillations reproduces the observed scaling of temporal broadening with distance and observing wavelength. For nearby pulsars, an empirical form of the model suggests that pulsars should show fine structure with significant modulation index in their scintillation spectra, over a range of bandwidths smaller than their fundamental decorrelation bandwidth  $\Delta\nu = 1/(2\pi\tau_s)$ . For pulsars PSR J0437-4715 and PSR B0950+08 the observed fundamental decorrelation bandwidth is an order of magnitude or more below the fine structure observed at higher frequencies, and previously identified erroneously as the fundamental decorrelation bandwidth.

We propose that similar, wider “fundamental” decorrelation bandwidths may be found for other low-DM pulsars. The model suggests that the angular broadening of such pulsars might be less than that expected on the basis of their higher-frequency scintillation spectra, as observed (Britton, Gwinn, & Ojeda 1998). Moreover, the model explains in a natural way the

fine structure seen in the scintillation spectra of some of these pulsars (Stinebring et al. 2001). Finally, the model may explain the extreme scattering events (isolated events of extremely large scattering by individual structures in the interstellar medium) seen for compact radio sources and pulsars (Fiedler et al. 1987; Cognard et al. 1993; Kedziora-Chudczer et al. 1997). Additional aspects of the model that remain to be explored further are the prevalence and scaling of fine structure for nearby pulsars, analogous structure for more distant pulsars, and searches for fine structure in temporal broadening and interferometric observations. Theoretical studies of the prevalence of fine structure and its expected effects in spectral, time-broadening, and interferometric observations, and of the origin of the Levy distribution in a model for turbulence in the ISM, are also essential to evaluating the model.

We thank A. Deshpande and N. Issur for helpful communications of their observations of PSR J0437-4715, and the National Science Foundation for financial support.

## REFERENCES

Armstrong, J. W., & Rickett, B. J. 1981, MNRAS, 194, 623

Bell, J. F., Bailes, M., Manchester, R. N., Weisberg, J. M., & Lyne, A. G. 1995, ApJ, 440, L81

Bhat, N. D. R., Rao, A. P., & Gupta, Y. 1999, ApJS, 121, 483

Boldyrev, S., & Gwinn, C. R. 2002, submitted to ApJ

Britton, M. C., Gwinn, C. R., & Ojeda, M. J. 1998, ApJ, 501, L101

Britton, M. C. 1997, Ph.D. thesis, University of California, Santa Barbara

Cognard, I., Bourgois, G., Lestrade, J.F., Biraud, F., Aubry, D., Darchy, B., & Drouhin, J. P. 1993, Nature, 366, 320

Cordes, J. M., Weisberg, J. M., & Boriakoff, V. 1985, ApJ, 288, 221

Cordes, J. M. 1986, ApJ, 311, 183

Cordes, J. M., & Wolszczan, A. 1986, ApJ, 307, L27

Desai, K. M., Gwinn, C. R., Reynolds, J. R., King, E. A., Jauncey, D., Flanagan, C., Nicolson, G., Preston, R. A., & Jones, D. L. 1992, ApJ, 393, L75

Fiedler, R.L., Dennison, B., Johnston, K.J., & Hewish, A., 1987, *Nature*, 326, 675

Frisch, U. 1995, *Turbulence: the Legacy of A.N. Kolmogorov*, (Cambridge: Cambridge University Press)

Fruchter, A. S. 1998, <http://icarus.stsci.edu/~fruchter/nebula/nebula.html>

Gothoskar, P., & Gupta, Y. 2000, *ApJ*, 531, 345

Gupta, Y., Rickett, B. J., & Lyne, A. G. 1994, *MNRAS*, 269, 1035

Gupta, Y. 1995, *ApJ*, 451, 717

Gupta, Y., Bhat, N. D. R., & Rao, A. P. 1999, *ApJ*, 520, 173

Gwinn, C. R., Britton, M. C., Reynolds, J. E. J., Jauncey, D. L., King, E. A., McCulloch, P. M., Lovell, J. E., & Preston, R. A. 1998, *ApJ*, 505, 928

Harrison, P. A., & Lyne, A. G. 1993, *MNRAS*, 265, 778

Isaacman, R., & Rankin, J. M. 1977, *ApJ*, 214, 214

Issur, N. 2000, Ph.D. thesis, University of Mauritius

Johnston, S., Nicastro, L., & Koribalski, B. 1998, *MNRAS*, 297, 108

Kedziora-Chudczer, L., Jauncey, D. L., Wieringa, M. H., Walker, M. A., Nicolson, G. D., Reynolds, J. E., & Tzioumis, A. K. 1997, *ApJ*, 490, L9

Lambert, H. C., & Rickett, B. J. 1999, *ApJ*, 517, 299

Lyne, A. G., & Graham-Smith, F. 1998, *Pulsar Astronomy*, (2nd ed.; Cambridge: Cambridge University Press)

Lyne, A. G., & Smith, F. G. 1982, *Nature*, 298, 825

Lyne, A. G., & Thorne, D. J. 1975, *MNRAS*, 172, 97

Nicastro, L., & Johnston, S. 1995, *MNRAS*, 273, 122

Phillips, J. A., & Clegg, A. W. 1992, *Nature*, 360, 137

Roberts, J. A., & Ables, J. G. 1982, *MNRAS*, 201, 1119

Sandhu, J. S., Bailes, M., Manchester, R. N., Navarro, J., Kulkarni, S. R., & Anderson, S. B. 1997, *ApJ*, 478, L95

Smirnova, T. V., & Shabanova, T. 1992, Soviet Astron., 36, 628

Stinebring, D. R., McLaughlin, M. A., Cordes, J. M., Becker, K. M., Espinoza Goodman, J. E., Kramer, M. A., Sheckard, J. L., & Smith, C. T. 2001, ApJ, 549, L97

Sutton, J. M., 1971, MNRAS, 155, 51

Taylor, J. H., & Cordes, J. M. 1993, ApJ, 411, 674

Taylor, J. H., Manchester, R. N., & Lyne, A. G. 1993, ApJS, 88, 529

Thompson, A. R., Moran, J. M., & Swenson, G. W., Jr. 1986, Interferometry and Synthesis in Radio Astronomy, (New York: John Wiley & Sons)

Toscano, M., Sandhu, J. S., Bailes, M., Manchester, R. N., Britton, M. C., Kulkarni, S. R., Anderson, S. B., & Stappers, B. W. 1999, MNRAS, 307, 925

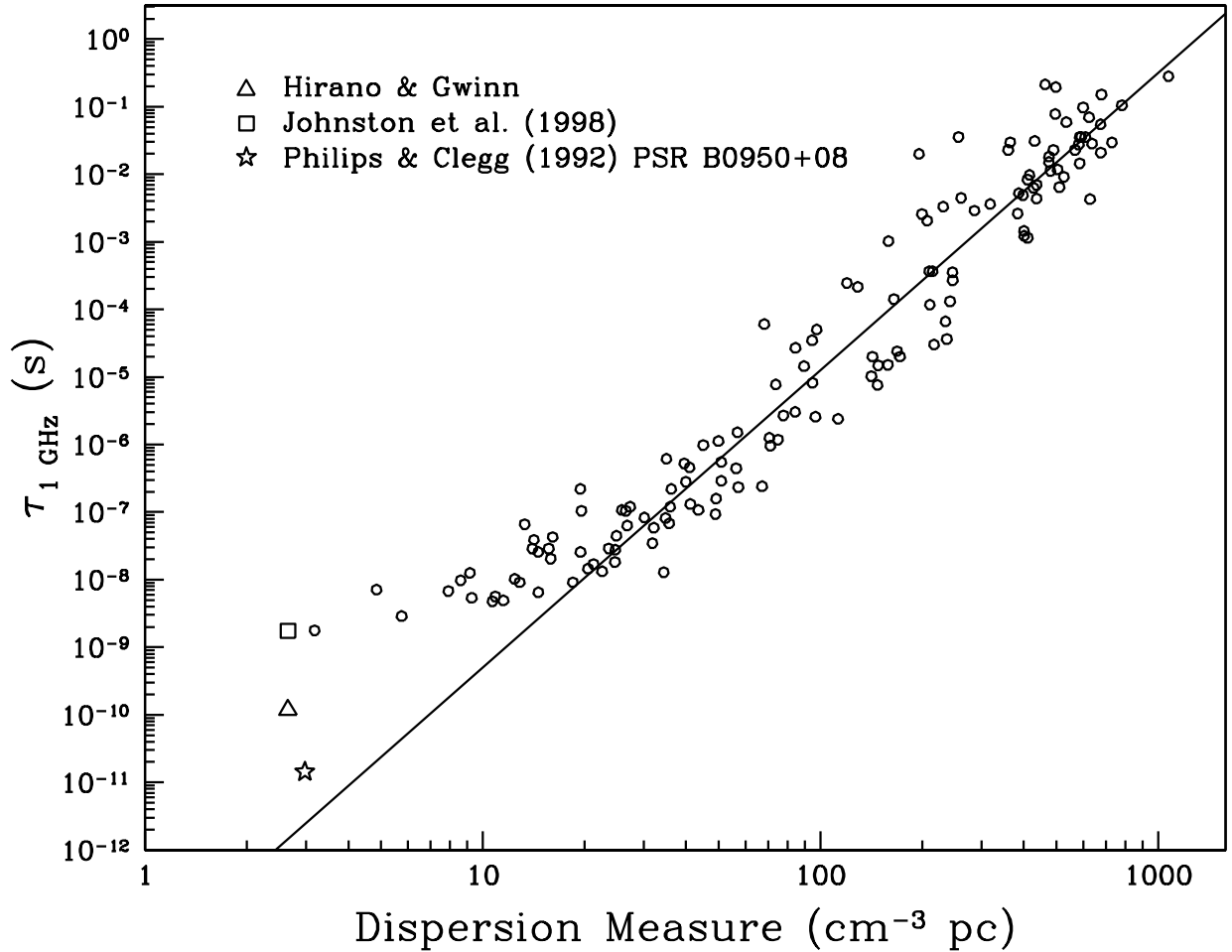


Fig. 1.— The relationship between temporal broadening and dispersion measure. The line, fitted by eye, has a slope of 4.4. Except as noted, the data were taken from Taylor, Manchester, & Lyne (1993).

Fig. 2.— **Please see Figure 2 in file f2.png** These plots show the visibility amplitude as a function of frequency and time for observations of PSR J0437-4715 on the Fort Davis-Pie Town baseline on 5 November 1996 (bottom) and 8 April 1999 (top).

Fig. 3.— **Please see Figure 3 in file f3.png** A contour plot of the two-dimensional ACF amplitude obtained for the Fort Davis-Pie Town baseline.

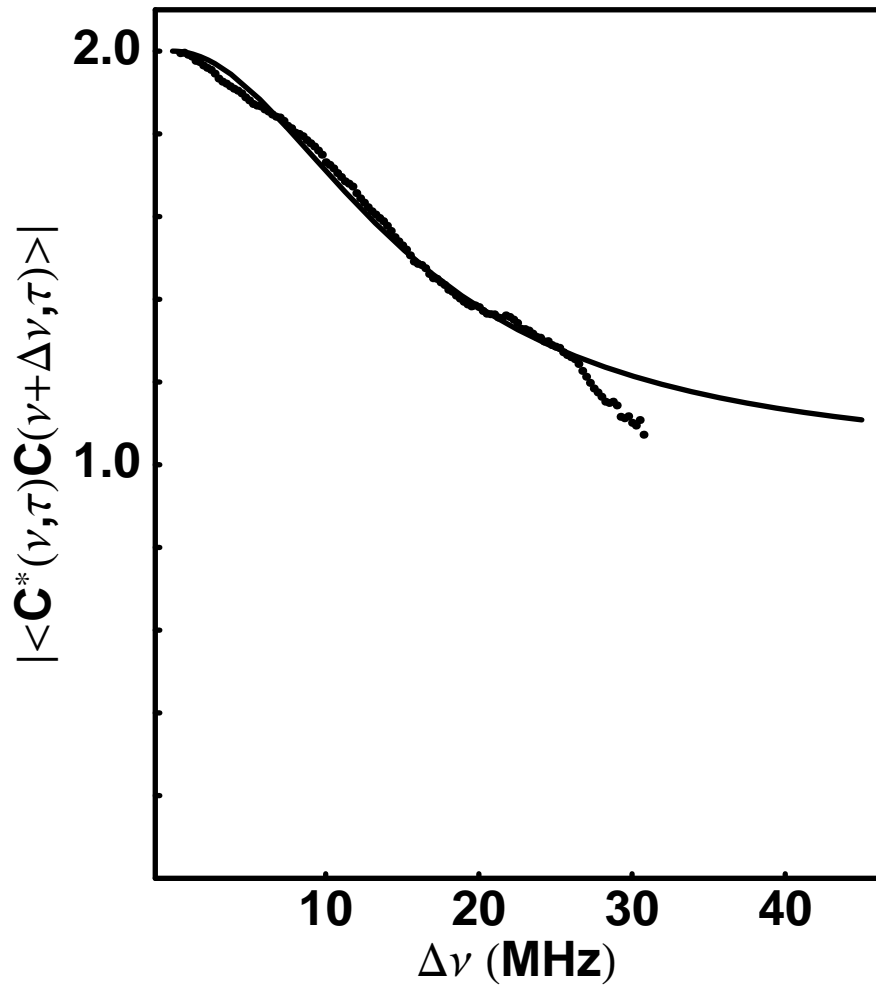


Fig. 4.— The composite ACF obtained by suitably combining the ACFs from the two observations. The best-fitting Lorentzian has a characteristic width of  $\Delta\nu_{ISS} = 15.7 \pm 0.2$  MHz.

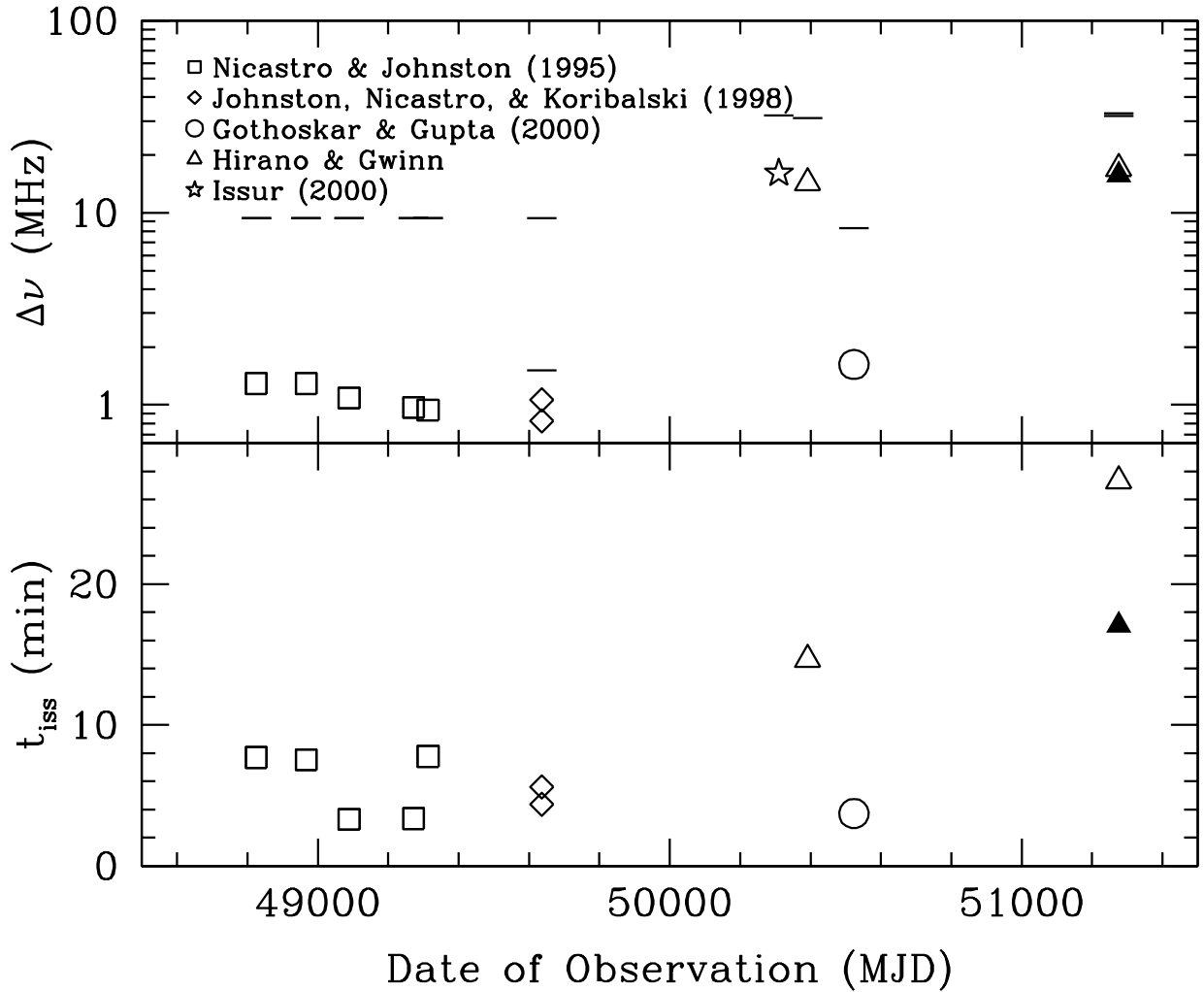


Fig. 5.— Measurements of the decorrelation bandwidth and scintillation time scale plotted against observing date. The horizontal lines indicate the effective bandwidth used for each measurement. The solid triangles show our estimates of  $\Delta\nu_{ISS}$  and  $t_{ISS}$  derived from the composite ACF.

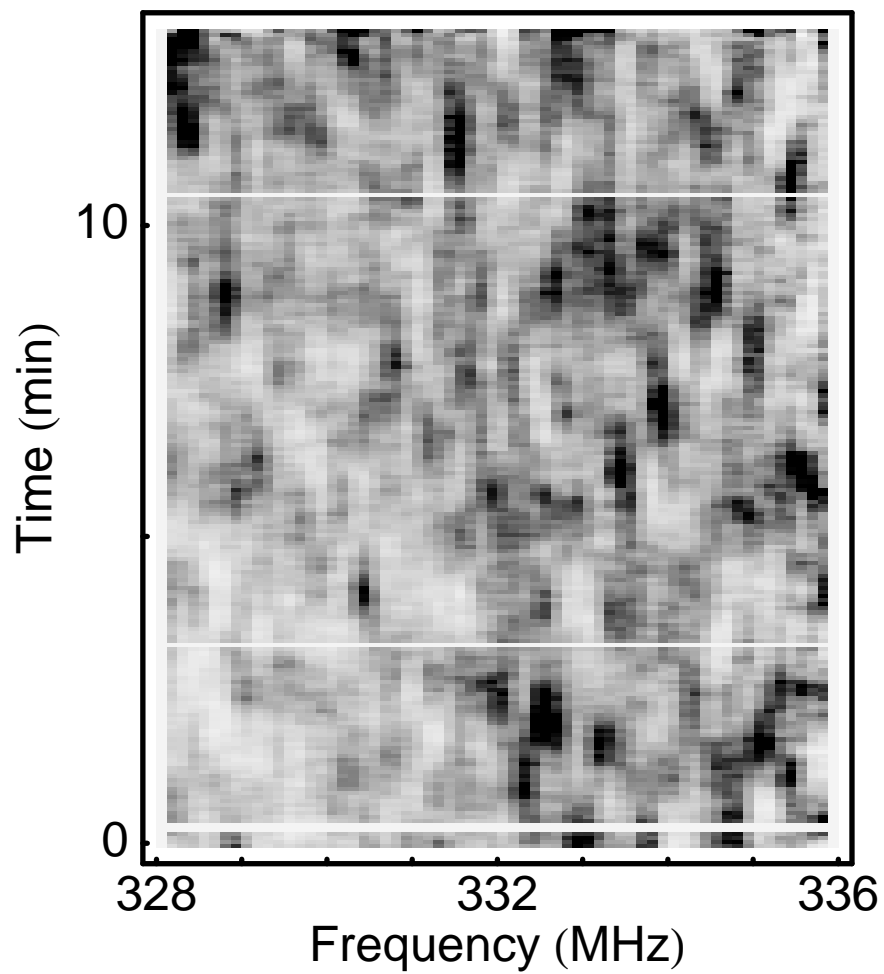


Fig. 6.— Variations in the visibility amplitude within a scintillation maximum appear to occur over a frequency scale on the order of 1 MHz.

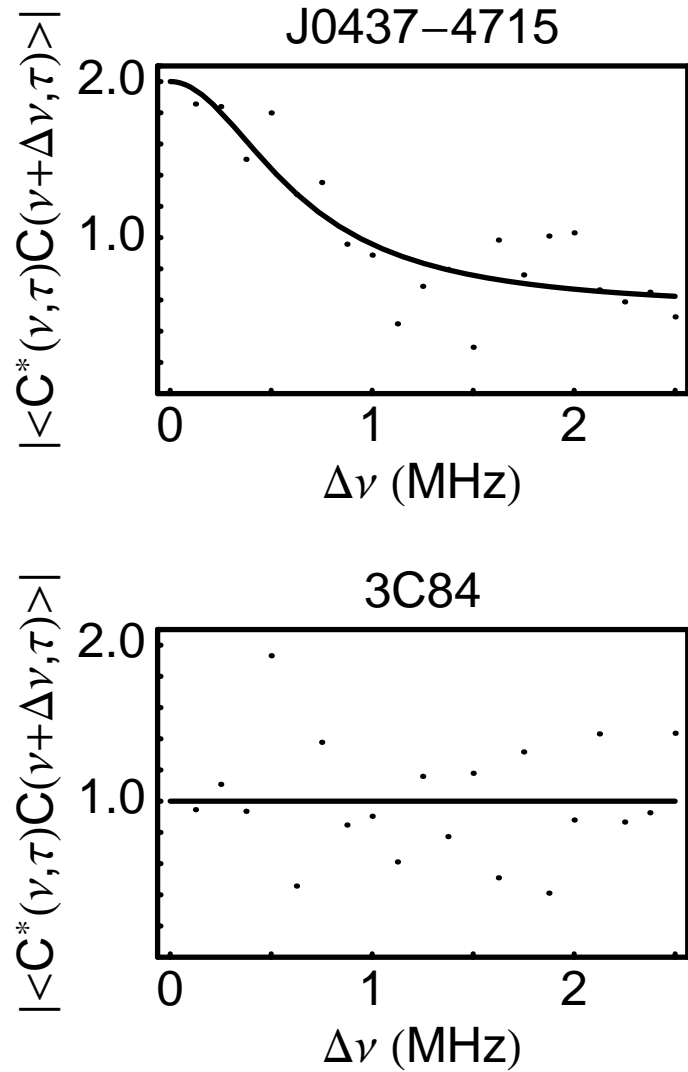


Fig. 7.— An autocorrelation function calculated for a portion of the pulsar (upper) data reveals correlations for small frequency lags of order 0.6 MHz. The autocorrelation function for calibrator source 3C84 (lower), in contrast, exhibits no correlations.

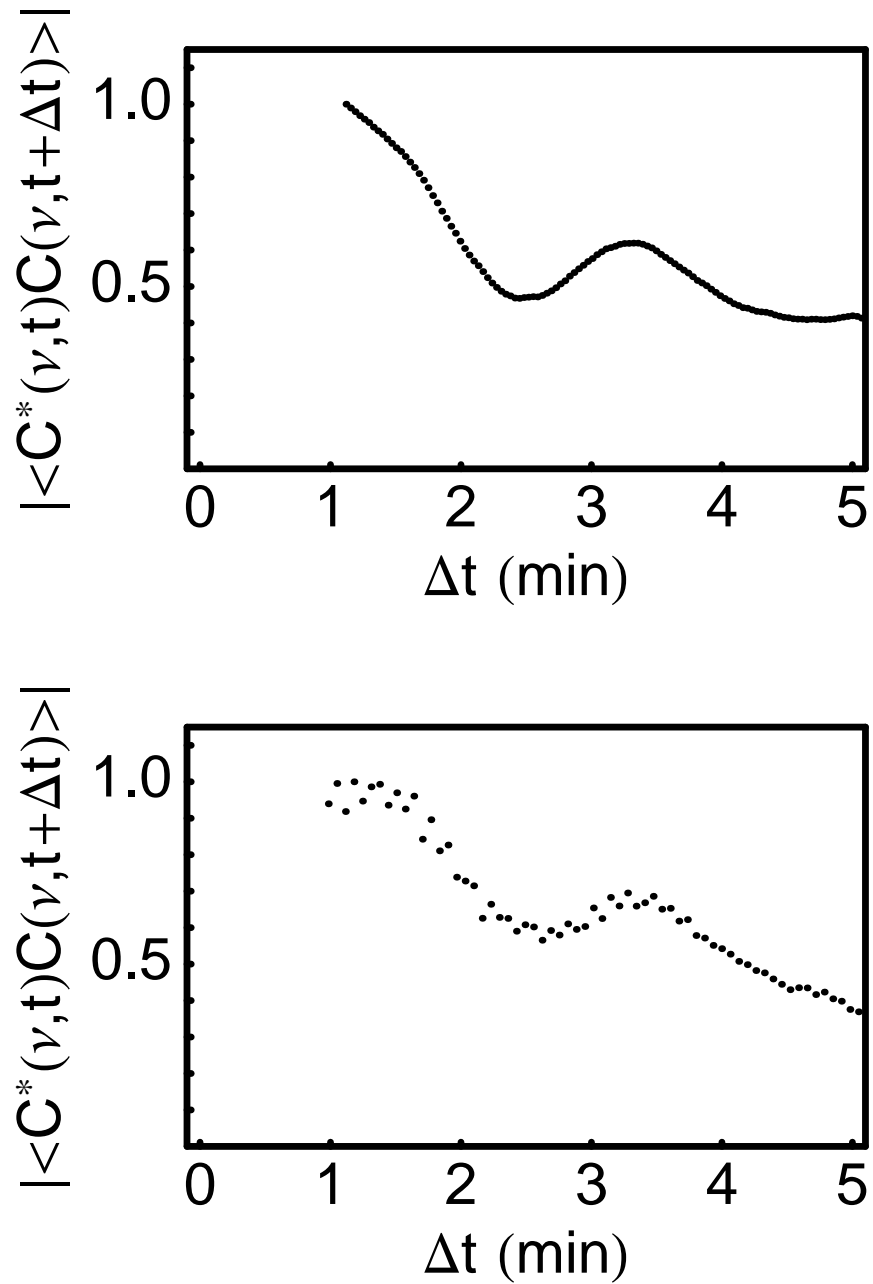


Fig. 8.— The time-domain autocorrelation functions for the maxima from the first (upper) and second (lower) epochs reveal correlation on a time scale of one to two minutes.

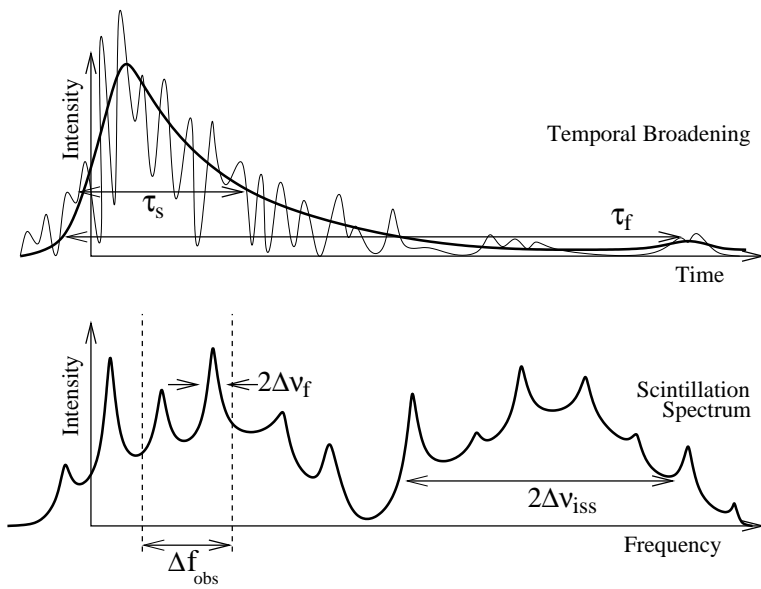


Fig. 9.— Schematic view of effects in the frequency and time domains of intermittent, large-angle scattering. This scattering may be evidence of non-Gaussian density fluctuations described by Levy statistics. Upper: Time-broadened shape of a narrow pulse. The average shape is smooth (bold line). Constructive and destructive interference of paths of different lengths creates a complicated shape for an originally very narrow pulse (narrow line). The “fundamental” scale of temporal broadening from multiple scattering is  $\tau_s$ . Large deflections lead to the longer delays such as  $\tau_f$ . Lower: Scintillation spectrum, showing broad features with decorrelation bandwidth  $\Delta\nu_{ISS} = 1/(2\pi\tau_s)$ , and narrowband structures corresponding to rare, large deflections with bandwidth  $\Delta\nu_f = 1/(2\pi\tau_f)$ . Observations with instrumental bandwidth  $\Delta f_{obs}$  are likely to find a scintillation bandwidth  $\Delta\nu_f$ .

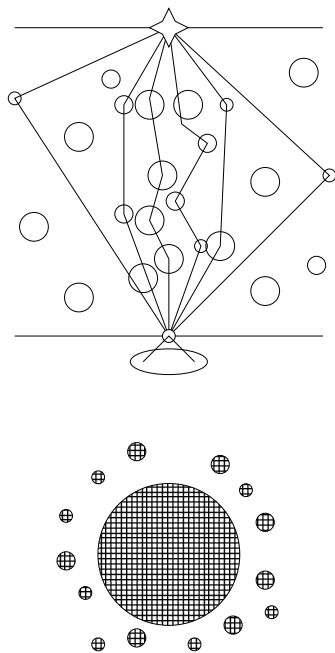


Fig. 10.— Upper: Schematic view of interstellar radio-wave propagation from the source at top to the observer's telescope at bottom. At small angles, the cumulative effect of many small deflections produce optically-thick scattering, whereas at large angles, individual large deflections produce optically-thin scattering. Lower: Schematic view of the resulting scattered image, filled from optically-thick scattering at center, surrounded with outlying paths from optically-thin scattering by single large deflections .

This figure "f2.png" is available in "png" format from:

<http://arxiv.org/ps/astro-ph/0204367v1>

This figure "f3.png" is available in "png" format from:

<http://arxiv.org/ps/astro-ph/0204367v1>